ACS APPLIED MATERIALS & INTERFACES

Research Article

www.acsami.org

Hierarchical α-Fe_2O_3/NiO Composites with a Hollow Structure for a Gas Sensor

Chen Wang,[†] Xiaoyang Cheng,[†] Xin Zhou,[†] Peng Sun,*[,†] Xiaolong Hu,[†] Kengo Shimanoe,[‡] Geyu Lu,*[,†] and Noboru Yamazoe[‡]

[†]State Key Laboratory on Integrated Optoelectronics, College of Electronic Science and Engineering, Jilin University, Changchun 130012, People's Republic of China

[‡]Department of Energy and Material Sciences, Faculty of Engineering Sciences, Kyushu University, Kasuga-shi, Fukuoka 816-8580, Japan

Supporting Information

ABSTRACT: Hierarchical α-Fe_2O_3/NiO composites with a hollow nanostructure were synthesized by a facile hydrothermal method. The structures and morphologies of the composites were investigated by different kinds of techniques, including X-ray diffraction, field-emission electron scanning microscopy, transmission electron microscopy, and energy dispersive spectroscopy. Hierarchical α-Fe_2O_3/NiO composites were fabricated by growing the α-Fe_2O_3 nanorods on the surfaces of porous NiO nanosheets with a thickness of ~12 nm. The gas sensing properties of hierarchical α-Fe_2O_3/NiO composites toward toluene were investigated using a static system. The response of α-Fe_2O_3/NiO composites to 100 ppm toluene was ~18.68, which was 13.18 times higher than that of pure NiO at 300 °C. The enhanced response can be attributed to heterojunction. Meanwhile, the rapid response and recovery characteristics were observed because of the porous hollow structural characteristics and catalytic actions of α-Fe_2O_3 and NiO.

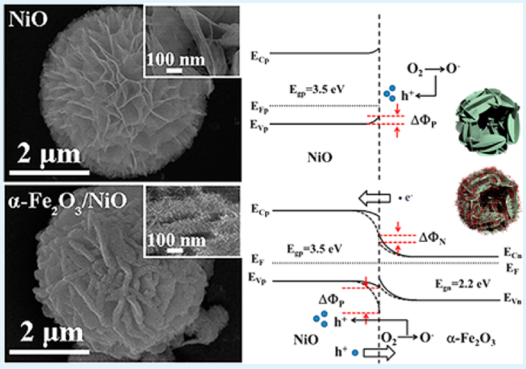

KEYWORDS: *α-Fe_2O_3/NiO composites, hollow nanostructure, hydrothermal, gas sensor, heterojunction*

INTRODUCTION

For the purpose of environmental monitoring and detection of inflammable, explosive, or toxic gases, oxide semiconductor gas sensors have been investigated extensively.[1−3] The development of new sensor strategies for ever-increasing sensitivity, accelerating response and recovery rate, and improving selectivity represents one of the major scientific challenges because high sensitivity, rapid response, and excellent selectivity are the three most important parameters for oxide semiconductor gas sensors. Over the past few decades, metal oxide semiconductors such as SnO_2,[4] WO_3,[5] In_2O_3,[6] ZnO,[7] and α-Fe_2O_3[8] have been widely investigated as sensing materials, because of their strong response to the target gases and simplicity of synthesis. For semiconductor gas sensors, the most widely accepted sensing mechanism can be explained by the change in resistance caused by the adsorption of oxygen and reaction with test gas molecules on the surface. Therefore, the gas sensing properties of oxide semiconductors are closely related to their composition, crystalline size, and surface morphology. Recently, many studies have demonstrated that oxide semiconductor composites, which consist of chemically distinct components, show more excellent sensing properties than a single oxide.[9−12] It has been established that the sensing properties of these composites are strongly dependent on their architectures, so the design and synthesis of composites with novel architectures still have important scientific and practical significance.

Nickel oxide (NiO) and hematite (α-Fe_2O_3), as two kinds of important functional materials, have received extensive attention because of their unique physical and chemical properties, which have led to their excellent performance in a broad range of applications involving catalysis,[13,14] gas sensors,[15,16] electrodes,[17,18] magnetic materials,[19,20] electrochemical supercapacitors,[21,22] etc. Considering the wide use of NiO and α-Fe_2O_3 as catalysts to promote selective oxidation of multifarious volatile organic compounds,[13,14] oxidizabilities stronger than those of SnO_2, WO_3, etc., and the different conductive types (NiO, p-type; α-Fe_2O_3, n-type), we integrated them together aiming to fabricate a new promising material for improving the gas sensing performance of toluene. For these reasons, nanostructures of NiO and α-Fe_2O_3 with various morphologies[23−34] have been obtained by a number of different methods, including the hydrothermal method,[35,36] the pulsed laser deposition method,[37] the solution plasma method,[38] the

Received: February 20, 2014
Accepted: July 9, 2014
Published: July 9, 2014

microemulsion method,[39] and the hard-template method.[40] Among them, the solution-phase route is regarded as an economic alternative way to synthesize oxides with the advantages of being a low-cost, mild, and more controllable method in the reaction process. Despite these exciting results, to the best of our knowledge, studies of hierarchical α-Fe_2O_3/NiO composites with a hollow structure synthesized by a template-free hydrothermal route have been rarely reported.

Herein, we present a strategy for synthesizing hierarchical α-Fe_2O_3/NiO composites with a well-defined morphology. The approach was based on two-step hydrothermal reactions. First, the three-dimensional flowerlike hierarchical NiO microspheres with a hollow structure were prepared via a hydrothermal route. Afterward, the one-dimensional (1D) α-Fe_2O_3 nanorods with a diameter of ~10 nm and a length of ~35 nm were assembled on the surfaces of NiO nanosheets by a facile hydrothermal process. Moreover, in comparison with pure urchinlike α-Fe_2O_3 hollow spheres and flowerlike NiO hollow microspheres, the enhanced gas sensing performance of hierarchical α-Fe_2O_3/NiO composites successfully demonstrates their potential application as the sensing material of a superior gas sensor.

EXPERIMENTAL SECTION

Preparation of Flowerlike Hierarchical NiO Microspheres. All the reagents were analytical grade and were used as received without further purification. The pure flowerlike NiO microspheres were synthesized by a hydrothermal reaction. In a typical experiment, 0.475 g of $NiCl_2{\cdot}6H_2O$ and 0.281 g of hexamethylenetetramine (HMT) were dissolved in a 30 mL mixed solution, which contained 15 mL of deionized water and 15 mL of ethanol, under vigorous stirring to form a homogeneous solution. Then 4 mL of ethanolamine (EA) was dropped into this solution that was stirred continuously until the color of the solution turned into clarified blue. Then, the obtained homogeneous solution was transferred into a 40 mL Teflon-lined stainless-steel autoclave and kept at 160 °C for 12 h. Then the autoclave was cooled to room temperature naturally, and the resultant green precipitate was carefully collected and washed by centrifugation with deionized water and ethanol several times before being dried at 80 °C in air for 10 h. Finally, the gray-black flowerlike hierarchical NiO hollow microspheres were obtained after annealing above the green precipitate at 350 °C for 1 h in air.

Preparation of Hollow Hierarchical α-Fe_2O_3/NiO Composites. The hierarchical α-Fe_2O_3/NiO composites were synthesized via a facile hydrothermal process. In brief, 10 mg of the obtained NiO powders mentioned above was dispersed in 16 mL of deionized water under vigorous stirring. Then, 8.6 mg of $FeCl_3{\cdot}6H_2O$ and 10.3 mg of $Na_2SO_4{\cdot}10H_2O$ were added to the suspension described above. Afterward, the mixture was poured into a 40 mL Teflon-lined stainless-steel autoclave and heated at 120 °C for 2.5 h. After the autoclave had cooled to room temperature, the resulting products were centrifuged, washed with deionized water and ethanol, and dried at 80 °C in air for 10 h. Eventually, the α-Fe_2O_3/NiO composites were obtained after calcining at 450 °C for 2 h.

Characterization. The structures of the materials were investigated using X-ray diffraction on a Rigaku TTRIII X-ray diffractometer (using Cu Kα radiation at a wavelength of 1.5406 Å), and the data were collected from 20° to 80°. The morphologies were observed by field emission scanning electron microscopy (FESEM) on a JSM-7500F (JEOL) microscope operating at 15 kV. Transmission electron microscopy (TEM) and high-resolution TEM images were recorded on a JEM-2200FS instrument (JEOL) operating at 200 kV. The energy dispersive X-ray spectrometry (EDS) result was measured by the TEM attachment. The specific surface area was estimated using the Brunauer–Emmett–Teller (BET) equation based on the nitrogen adsorption isotherm obtained with a Micromeritics Gemini VII apparatus (Surface Area and Porosity System). The operating temperature was measured by the thermal infrared imager (FLIR T440).

Fabrication and Measurement of the Gas Sensor. The structure of the sensor is shown in Figure 1. A pair of Au electrodes

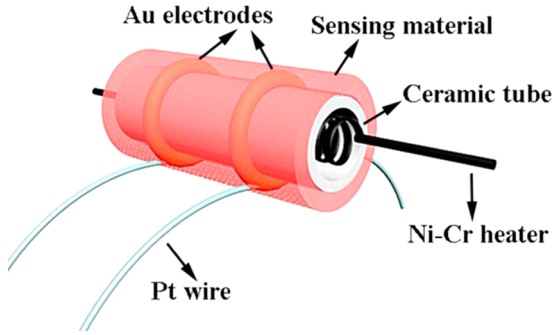

Figure 1. Schematic diagram of the gas sensor.

was installed at each end of the ceramic tube (4 mm in length, 1.2 mm in external diameter, and 0.8 mm in internal diameter). Each electrode was connected with two Pt wires. The NiO or α-Fe_2O_3/NiO composites powder was dispersed in deionized water to form a slurry, and then each powder was coated on the ceramic tube to form a thick sensing film. A Ni–Cr alloy coil heater was inserted into the alumina tube. The operating temperature was controlled by adjusting the heating current that passed through the heater. The gas sensing performance of the gas sensor was investigated using a static system. The sensors were put into an airtight chamber (50 L in volume) purged with pure air, and then a given amount of test gases was injected into the airtight chamber using a microsyringe for the measurement of the sensitive performance. The gas response of the sensor was defined as R_g/R_a (p-type) or R_a/R_g (n-type), where R_a is the electrical resistance of the gas sensor in air and R_g the resistance in the presence of target gases. The response and recovery times were defined as the time taken by the sensor to achieve 90% of the total resistance change in the case of adsorption and desorption, respectively.

RESULTS AND DISCUSSION

Structural and Morphological Characteristics. Powder X-ray diffraction (XRD) was conducted to identify the composition and crystalline phase of the final products. Panels a and b of Figure 2 show the XRD patterns of the as-synthesized flowerlike NiO microspheres and the composite oxides composed of NiO and α-Fe_2O_3, respectively. It is clear that in the first step hydrothermally synthesized and calcined products were matched well with the face-centered cubic phase of NiO (JCPDS Card No. 47-1049). After the crystallite size of the as-synthesized material had been calculated with the Scherrer formula, the NiO indicated an average crystallite size of 12 nm. In terms of the composites, the residual diffraction peaks were consistent with the rhombohedral structure of α-Fe_2O_3 (JCPDS Card No. 33-0664). No other diffraction peaks corresponding to impurities were observed, which indicated that the final product was a mixture of NiO and α-Fe_2O_3 with high purity.

The morphology of as-synthesized pure NiO was observed by FESEM and TEM. As shown in Figure 3a, the flowerlike NiO microspheres had good dispersivity and a uniform diameter of ~4 μm. Further observing a single flowerlike NiO microsphere in the inset of Figure 3a, we can find that the microsphere was assembled by many curving two-dimensional nanosheets. NiO nanosheets had rough and porous surfaces, and the thickness was ~12 nm, which can be clearly observed in

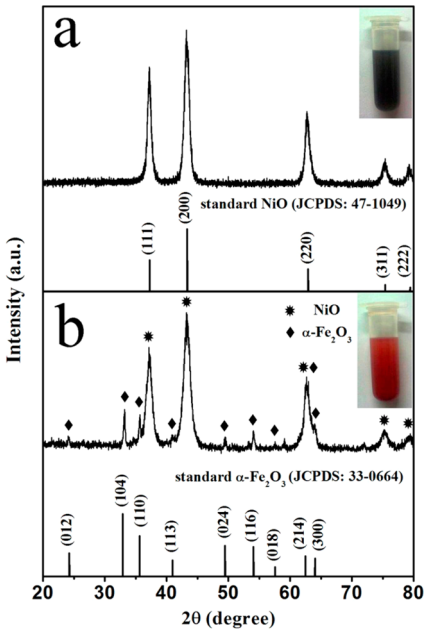

Figure 2. XRD patterns of the as-prepared flowerlike NiO (a) and hierarchical α-Fe_2O_3/NiO composites (b).

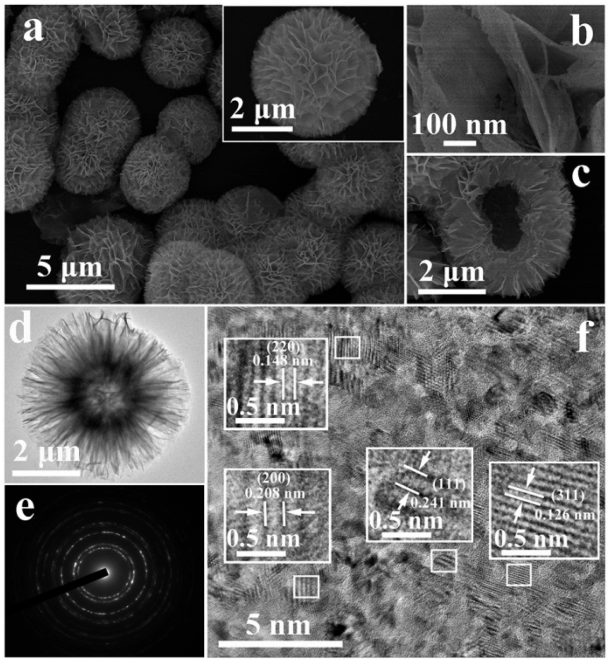

Figure 3. (a) Typical FESEM image of NiO microspheres. (b and c) High-magnification FESEM images. (d) Typical TEM image of a NiO sphere. (e) Corresponding SAED pattern. (f) HRTEM image.

Figure 3b. The hollow structure can be verified by a cracked flowerlike microsphere, and the inner diameter of the microsphere was ~1 μm, as displayed in Figure 3c. The typical TEM image of a single flowerlike NiO microsphere shown in Figure 3d further demonstrates that the products have a hollow spherical structure, which was similar to the FESEM observation. Figure 3e is the selected area electron diffraction (SAED) pattern of a part of a single NiO nanosheet, in which a series of diffraction rings could be clearly observed. It indicated that the NiO nanosheet was polycrystalline. Figure 3f shows a high-resolution TEM (HRTEM) image of a piece of a cracked NiO nanosheet, which further reveals that the crystalline structure of a single nanosheet was composed of many smaller intraconnected grains with fringe spacings of 0.148, 0.208, 0.241, and 0.126 nm corresponding to the (220), (200), (111), and (311) planes of cubic NiO, respectively.

After the second step of the hydrothermal reaction, α-Fe_2O_3 nanorods grew outward on the surfaces of NiO nanosheets for the fabrication of α-Fe_2O_3/NiO hierarchical composites. Figure 4a is the low-magnification FESEM image, in which the

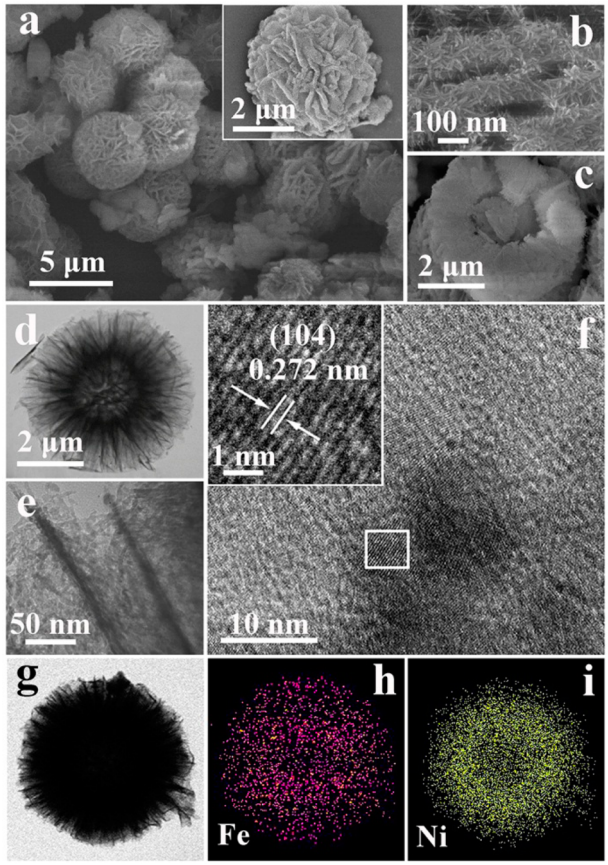

Figure 4. (a–c) Typical FESEM images of hierarchical α-Fe_2O_3/NiO composites. (d and e) Typical TEM images of composites. (f) HRTEM image. (g–i) Scanning TEM (STEM) image and corresponding elemental mapping images.

flowerlike microsphere architectures were maintained after the second hydrothermal process. However, many 1D nanorods grew on NiO nanosheets, resulting in the microspheres being turned into furry spheres, as shown in the inset of Figure 4a. Particularly observed from the enlarged magnification image (Figure 4b), the 1D α-Fe_2O_3 nanorods (~5 nm in diameter and 35 nm in length) were aligned in an unorderly fashion and radially oriented on each basal surface of the NiO nanosheets. Besides, the hollow structure of the flowerlike microspheres was maintained, which can be verified by a cracked sphere in Figure 4c, and the inner diameter of the microsphere was almost invariable. TEM and HRTEM were utilized to further investigate the structure of hierarchical α-Fe_2O_3/NiO composites. Figure 4d clearly shows the hollow structural feature of the products. According to the high-magnification TEM image (Figure 4e), the profile of NiO nanosheets could be clearly distinguished by the darker region and a large amount of α-Fe_2O_3 nanorods intricately grew on the both sides of the

profile, which appeared as a light color. Figure 4f presents a high-resolution TEM (HRTEM) image of α-Fe_2O_3 nanorods, which reveals that the nanorods were single-crystalline. The lattice fringes were clearly observed, and the fringe spacing was 0.272 nm, which was consistent with the interplanar spacing of (104) planes of rhombohedral α-Fe_2O_3. Figure 4g is the scanning TEM (STEM) image of a single microsphere. TEM elemental mapping was conducted to clearly confirm the spatial distribution of Ni and Fe in the flowerlike hierarchical composite structure. As shown in panels h and i of Figure 4, the signals of Ni were detected in the middle as a sphere shell with an obvious dark region in the center and the signals of Fe were detected uniformly in the whole sphere region. It indicated that the distribution of α-Fe_2O_3 on the NiO microspheres was very uniform. The EDS analysis (Figure S1 of the Supporting Information) further reflected the composites consisted of Ni, Fe, and O elements.

Gas Sensing Properties. It is well-known that the operating temperature is an important parameter for a semiconductor oxide sensor. The gas response is highly dependent on the operating temperature. Figure 5a shows

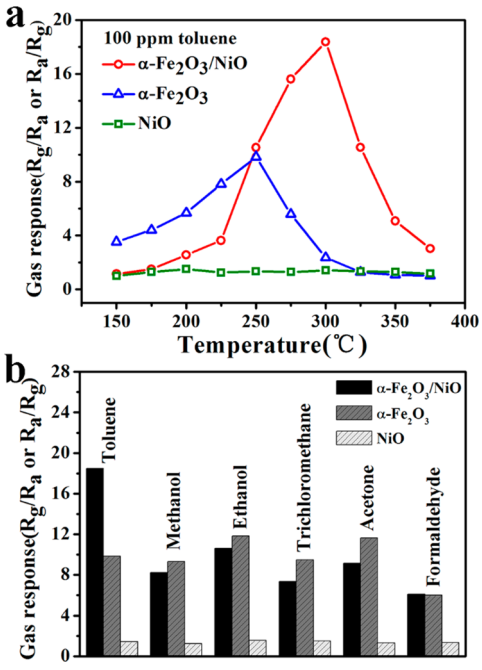

Figure 5. (a) Responses of pure NiO, α-Fe_2O_3, and α-Fe_2O_3/NiO composites vs operating temperature to 100 ppm of toluene. (b) Selectivities of pure NiO, α-Fe_2O_3, and α-Fe_2O_3/NiO composites to 100 ppm of various gases.

the responses of the sensors based on α-Fe_2O_3/NiO composites, pure urchinlike α-Fe_2O_3 hollow spheres (the detailed synthesized process is shown in the Supporting Information, and the XRD pattern and FESEM image are shown in Figure S2 of the Supporting Information), and flowerlike NiO microspheres to 100 ppm of toluene at different operating temperatures to determine the optimal operating temperature. Obviously, the responses of the testing sensors changed with the operating temperature. The response of the sensor based on α-Fe_2O_3/NiO composites to 100 ppm of toluene increased rapidly with an increase in the operating temperature to 300 °C and then decreased with a further increase in the operating temperature. As a consequence, the response of the sensor based on α-Fe_2O_3/NiO composites to 100 ppm of toluene reached its maximum of 18.68 at 300 °C (the optimal operating temperature). Similar behavior could be observed in the case of the sensors based on pure urchinlike α-Fe_2O_3 hollow spheres and flowerlike NiO microspheres. However, their maximal responses appeared at different temperatures, and the values were much lower than those of α-Fe_2O_3/NiO composites. The response of the sensor based on pure α-Fe_2O_3 to 100 ppm of toluene reached the maximum of 9.84 at 250 °C, and that of pure NiO was 1.50 at 200 °C. Obviously, there were shifts of the optimal operating temperatures among α-Fe_2O_3/NiO composites, pure urchinlike α-Fe_2O_3 hollow spheres, and flowerlike NiO microspheres. It can be attributed to the differences in α-Fe_2O_3 and NiO on the catalytic oxidation of toluene at different temperatures. Moreover, the response of α-Fe_2O_3/NiO composites to 100 ppm of toluene was nearly 2 times higher than that of pure α-Fe_2O_3 and 13 times higher than that of pure NiO, which clearly suggested that the gas sensing response toward toluene was enhanced by fabricating the α-Fe_2O_3/NiO heterojunction.

The responses of three kinds of sensors to 100 ppm of various testing gases are shown in Figure 5b. The testing gases included toluene, methanol, ethanol, trichloromethane, acetone, and formaldehyde. Obviously, the sensor based on α-Fe_2O_3/NiO composites showed enhanced responses to toluene compared with those of pure α-Fe_2O_3 and NiO. Moreover, the sensor based on α-Fe_2O_3/NiO composites had the strongest response to toluene among the testing gases, and the response was 1.76−3.07 times higher than those for other testing gases, which revealed an excellent selectivity to toluene.

Because hierarchical α-Fe_2O_3/NiO composites were fabricated on a flowerlike NiO microsphere substrate and consistent with the sensing behavior of p-type semiconductor sensors, we further investigated the differences in gas sensing properties between α-Fe_2O_3/NiO composites and pure flowerlike NiO microspheres. The dynamic response characteristics of the sensors based on α-Fe_2O_3/NiO composites and pure flowerlike NiO microspheres to 100 ppm of toluene are shown in Figure S3 of the Supporting Information. The resistances of the sensors increased abruptly with the injection of the testing gas (toluene), decreased rapidly, and nearly recovered to their initial values after the testing gas was released. The response time of the sensor based on α-Fe_2O_3/NiO composites was 1 s to 100 ppm of toluene, and the recovery time was 12 s at 300 °C, which were shorter than those of the sensor based on pure NiO, whose response and recovery times were 5 and 17 s, respectively, under the same conditions, as shown in Figure S3a,c of the Supporting Information. The rapid response and recovery can be attributed to the porous hollow structure and the catalysis actions of NiO and α-Fe_2O_3 for the oxidation of toluene, which has been reported extensively in the literature.[13,41] The four reversible cycles of the response curve (Figure S3b,c of the Supporting Information) indicated stable and repeatable characteristics of as-fabricated sensors.

Figure 6 reveals the gas responses of two kinds of gas sensors as a function of the concentration of toluene at 300 °C. The results indicate that the gas responses of two kinds of sensors both increased with the increase in toluene concentration from 5 to 100 ppm. Obviously, the sensor based on α-Fe_2O_3/NiO composites exhibited a quite enhanced gas response compared with that of pure NiO. Panels b and c of Figure 6 show the dynamic response resistances of two kinds of sensors to different concentrations of toluene at 300 °C. The responses of

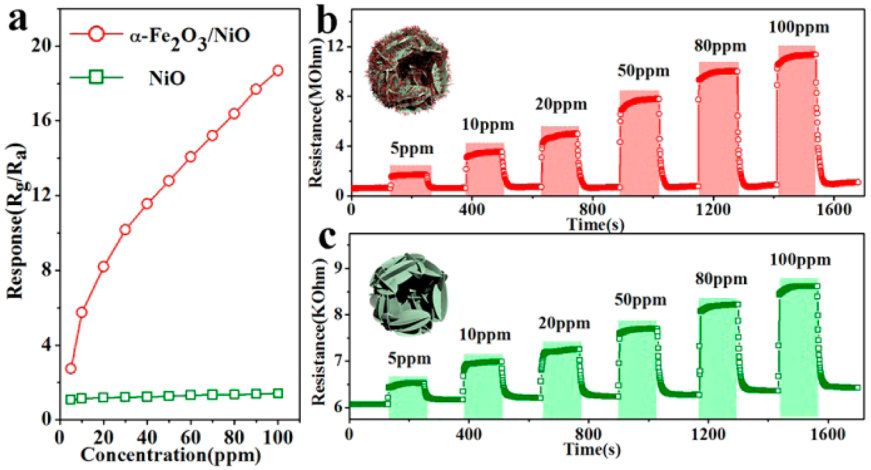

Figure 6. (a) Response of pure NiO and α-Fe_2O_3/NiO composites at 300 °C vs toluene concentration. (b and c) Dynamical response transients of the α-Fe_2O_3/NiO composites and pure NiO to different concentrations of toluene, respectively.

the sensor based on α-Fe_2O_3/NiO composites were approximately 2.74, 5.74, 8.18, 12.77, 16.38, and 18.68 to 5, 10, 20, 50, 80, and 100 ppm of toluene, respectively, while the responses of pure NiO were only 1.07, 1.15, 1.19, 1.27, 1.35, and 1.42, respectively, under the same condition. Evidently, the addition of α-Fe_2O_3 can effectively improve the response of the gas to toluene. Meanwhile, these two kinds of gas sensors exhibited excellent response and recovery characteristics with respect to different concentrations of toluene ranging from 5 to 100 ppm.

The long-term stability of the gas sensor is one of most important parameters in a practical application. As shown in Figure 7a, the gas response of the sensor based on α-Fe_2O_3/NiO composites to 100 ppm of toluene at 300 °C was nearly constant after 200 continuous cyclic tests, which suggested the α-Fe_2O_3/NiO microstructure had excellent robustness. Moreover, the response as a function of the number of testing days is also measured and shown in Figure 7b. The result further indicated the splendid long-term stability of the sensor based on α-Fe_2O_3/NiO composites.

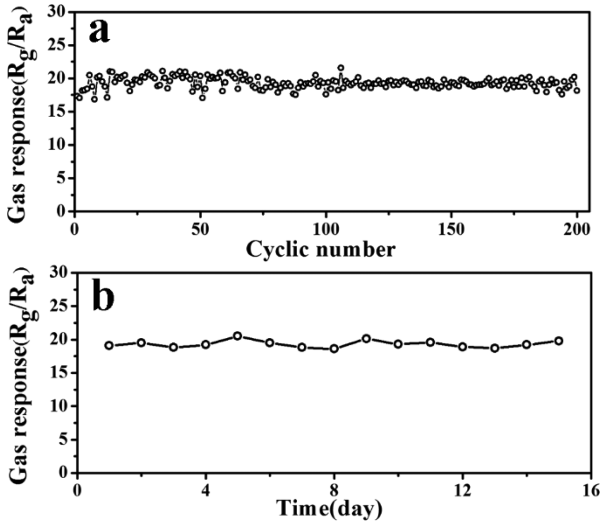

Figure 7. Responses of the sensor based on α-Fe_2O_3/NiO composites as a function of the number of (a) cyclic tests and (b) test days to 100 ppm of toluene at 300 °C.

Gas Sensing Mechanism. The sensing mechanism is based on the change in resistance of the sensor by the adsorption and desorption processes of oxygen molecules on the surface of oxides. In general, when a p-type metal oxide semiconductor gas sensor is exposed to air, oxygen molecules will be adsorbed onto the surfaces of the sensing materials and ionize into species such as O^{2-}, O^-, and O_2^- by transferring holes to the valence band of the p-type semiconductor. In this process, oxygen molecules act as hole donors to increase the hole concentration and decrease the resistance of the sensor. NiO is a p-type semiconductor with hole carriers, and the adsorption of the oxygen molecules causes the formation of the hole-accumulation layer on the surface of NiO, which results in the upward bending of the energy band near the surface, as shown in Figure 8b. Upon exposure to a toluene gas atmosphere at an appropriate temperature, these gas molecules will react with the adsorbed oxygen ions on the surface of NiO and release electrons to recombine with holes, which increase the resistance of the sensor.

The enhanced gas sensing properties of α-Fe_2O_3/NiO composites are likely to be a result of the following factors. First, the structural characteristics of hierarchical α-Fe_2O_3/NiO composites provide a high surface area and good permeability. The surface area of hierarchical α-Fe_2O_3/NiO composites (129.97 m^2 g^{-1}) is larger than that of pure flowerlike NiO (109.64 m^2 g^{-1}) (Figure S4 of the Supporting Information). This means that more oxygen can be absorbed and ionized. Meanwhile, the effective and rapid gas diffusion toward both the inner and surface regions of the hollow spheres can be easily accomplished because of the hollow structure, porous nanosheets, and large pores constituted by the space between nanosheets (Figure 8a). Therefore, a strong response and a short response time are obtained. Second, the p−n junction between NiO and α-Fe_2O_3 is the principal factor in the enhanced response of composites. Because the Fermi level of α-Fe_2O_3 is higher than NiO, electrons will flow from α-Fe_2O_3 to NiO while holes will flow along the contrary direction of electrons, which will result in the formation of the hole depletion layer (Figure 8c) and the increase in the amount of the adsorbed oxygen species. In this case, more electrons will be released back to the composites and the enhanced response will be obtained eventually. In addition, it is well-known that the lattice mismatch is unavoidable in the heterojunction. For this

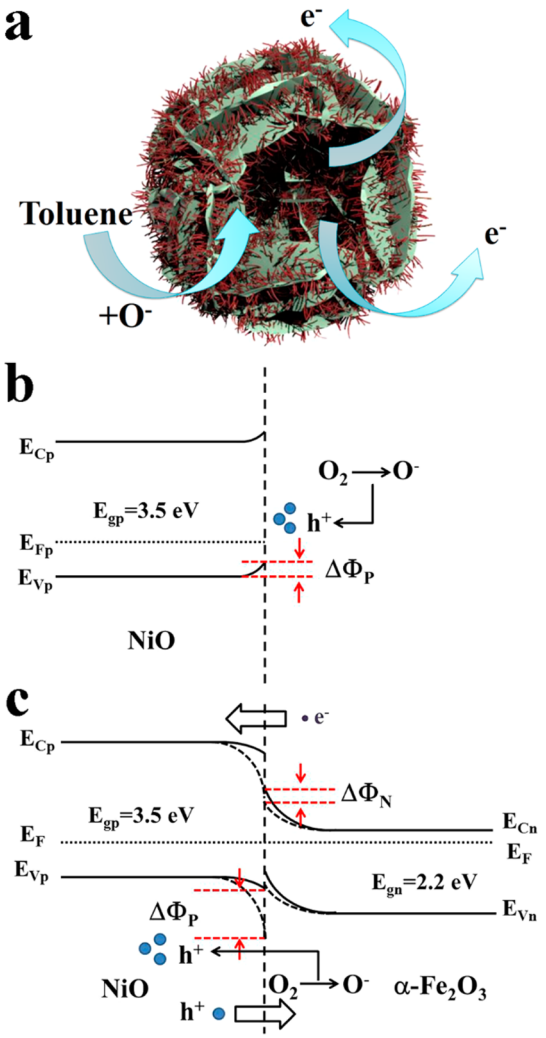

Figure 8. Schematic diagrams (a) illustrating the plausible reason for fast response and recovery and the energy band structure of (b) pure NiO and (c) α-Fe_2O_3/NiO heterostructures in air.

reason, a number of dangling bonds are produced in the material with a smaller lattice constant near the interface and form a large amount of interface states. For a p-type semiconductor, the dangling bonds perform an electron donor function. In our as-synthesized composites, NiO possesses a lattice constant smaller than that of α-Fe_2O_3; therefore, the number of holes in NiO decreases near the interface, which is beneficial to further increase the amount of adsorbed oxygen species. As a result of the reasons mentioned above, the heterojunction acts as a hole-pump machine. Therefore, the enhanced gas response can be mainly attributed to the formation of the heterojunction.

CONCLUSION

In summary, novel hierarchical composites composed of flowerlike NiO microspheres and α-Fe_2O_3 nanorod branches had been successfully synthesized using a facile solution route. As a proof-of-concept demonstration of the function, such α-Fe_2O_3/NiO composite material was used as the sensing material of a gas sensor. Enhanced sensing properties with respect to toluene were observed by comparison with those of pure α-Fe_2O_3 and NiO hollow structures. The effect of the heterojunction between NiO and α-Fe_2O_3, the porous hollow structural characteristics, and the catalytic actions of NiO and α-Fe_2O_3 for the oxidation of toluene are probably responsible for the enhanced gas sensing performance.

ASSOCIATED CONTENT

Supporting Information

Preparation of hollow urchinlike α-Fe_2O_3, energy dispersive spectrum of the hierarchical α-Fe_2O_3/NiO composites, XRD pattern and FESEM image of hollow urchinlike α-Fe_2O_3, response transient and four periods of the response curve of the sensor based on hierarchical α-Fe_2O_3/NiO composites and pure NiO to 100 ppm of toluene at 300 °C, and N_2 adsorption−desorption isotherms of pure NiO and hierarchical α-Fe_2O_3/NiO composites. This material is available free of charge via the Internet at http://pubs.acs.org.

AUTHOR INFORMATION

Corresponding Authors

*E-mail: spmaster2008@163.com. Telephone: +86-431-85167808. Fax: +86-431-85167808.
*E-mail: lugy@jlu.edu.cn.

Notes

The authors declare no competing financial interest.

ACKNOWLEDGMENTS

This work is supported by the National Natural Science Foundation of China (61074172, 61134010, and 61327804), the Program for Chang Jiang Scholars and Innovative Research Team in University (IRT13018), and the National High-Tech Research and Development Program of China (863 Program, 2013AA030902).

ABBREVIATIONS

XRD, X-ray diffraction
FESEM, field-emission electron scanning microscopy
TEM, transmission electron microscopy
EDS, energy dispersive spectroscopy
BET, Brunauer−Emmett−Teller
HMT, hexamethylenetetramine
EA, ethanolamine
SAED, selected area electron diffraction
HRTEM, high-resolution transmission electron microscopy
STEM, scanning transmission electron microscopy

REFERENCES

(1) Wetchakun, K.; Samerjai, T.; Tamaekong, N.; Liewhiran, C.; Siriwong, C.; Kruefu, V.; Wisitsoraat, A.; Tuantranont, A.; Phanichphant, S. Semiconducting Metal Oxides as Sensors for Environmentally Hazardous Gases. *Sens. Actuators, B* **2011**, *160*, 580−591.
(2) Gurlo, A. Nanosensors: Towards Morphological Control of Gas Sensing Activity. SnO_2, In_2O_3, ZnO and WO_3 Case Studies. *Nanoscale* **2011**, *3*, 154−165.
(3) Cao, B. B.; Chen, J. J.; Tang, X. J.; Zhou, W. L. Growth of Monoclinic WO_3 Nanowire Array for Highly Sensitive NO_2 Detection. *J. Mater. Chem.* **2009**, *19*, 2323−2327.
(4) Wang, Y. L.; Jiang, X. C.; Xia, Y. N. A Solution-Phase, Precursor Route to Polycrystalline SnO_2 Nanowires That Can Be Used for Gas Sensing under Ambient Conditions. *J. Am. Chem. Soc.* **2003**, *125*, 16176−16177.
(5) Vallejos, S.; Stoycheva, T.; Umek, P.; Navio, C.; Snyders, R.; Bittencourt, C.; Llobet, E.; Blackman, C.; Moniz, S.; Correig, X. Au Nanoparticle-Functionalised WO_3 Nanoneedles and Their Application

in High Sensitivity Gas Sensor Devices. *Chem. Commun.* **2011**, *47*, 565−567.
(6) Waitz, T.; Wagner, T.; Sauerwald, T.; Kohl, C.-D.; Tiemann, M. Ordered Mesoporous In_2O_3: Synthesis by Structure Replication and Application as A Methane Gas Sensor. *Adv. Funct. Mater.* **2009**, *19*, 653−661.
(7) Li, J.; Fan, H. Q.; Jia, X. H. Multilayered ZnO Nanosheets with 3D Porous Architectures: Synthesis and Gas Sensing Application. *J. Phys. Chem. C* **2010**, *114*, 14684−14691.
(8) Song, H.-J.; Jia, X.-H.; Qi, H.; Yang, X.-F.; Tang, H.; Min, C.-Y. Flexible Morphology-Controlled Synthesis of Monodisperse α-Fe_2O_3 Hierarchical Hollow Microspheres and Their Gas-Sensing Properties. *J. Mater. Chem.* **2012**, *22*, 3508−3516.
(9) Chu, D. W.; Zeng, Y.-P.; Jiang, D. L.; Masuda, Y. In_2O_3-SnO_2 Nano-Toasts and Nanorods: Precipitation Preparation, Formation Mechanism, and Gas Sensitive Properties. *Sens. Actuators, B* **2009**, *137*, 630−636.
(10) Sun, P.; Cai, Y. X.; Du, S. S.; Xu, X. M.; You, L.; Ma, J.; Liu, F. M.; Liang, X. S.; Sun, Y. F.; Lu, G. Y. Hierarchical α-Fe_2O_3/SnO_2 Semiconductor Composites: Hydrothermal Synthesis and Gas Sensing Properties. *Sens. Actuators, B* **2013**, *182*, 336−343.
(11) Yu, H.-L.; Li, L.; Gao, X.-M.; Zhang, Y.; Meng, F. N.; Wang, T.-S.; Xiao, G.; Chen, Y.-J.; Zhu, C.-L. Synthesis and H_2S Gas Sensing Properties of Cage-Like α-MoO_3/ZnO Composite. *Sens. Actuators, B* **2012**, *171*, 679−685.
(12) Aygun, S.; Cann, D. Response Kinetics of Doped CuO/ZnO Heterocontacts. *J. Phys. Chem. B* **2005**, *109*, 7878−7882.
(13) Bai, G. M.; Dai, H. X.; Deng, J. G.; Liu, Y. X.; Ji, K. M. Porous NiO Nanoflowers and Nanourchins: Highly Active Catalysts for Toluene Combustion. *Catal. Commun.* **2012**, *27*, 148−153.
(14) Zheng, Y. H.; Cheng, Y.; Wang, Y. S.; Bao, F.; Zhou, L. H.; Wei, X. F.; Zhang, Y. Y.; Zheng, Q. Quasicubic α-Fe_2O_3 Nanoparticles with Excellent Catalytic Performance. *J. Phys. Chem. B* **2006**, *110*, 3093−3097.
(15) Liu, B.; Yang, H. Q.; Zhao, H.; An, L. J.; Zhang, L. H.; Shi, R. Y.; Wang, L.; Bao, L.; Chen, Y. Synthesis and Enhanced Gas-Sensing Properties of Ultralong NiO Nanowires Assembled with NiO Nanocrystals. *Sens. Actuators, B* **2011**, *156*, 251−262.
(16) Sun, P.; Zhu, Z.; Zhao, P. L.; Liang, X. S.; Sun, Y. F.; Liu, F. M.; Lu, G. Y. Gas Sensing with Hollow α-Fe_2O_3 Urchin-Like Spheres Prepared via Template-Free Hydrothermal Synthesis. *CrystEngComm* **2012**, *14*, 8335−8337.
(17) Ma, J. M.; Yang, J. Q.; Jiao, L. F.; Mao, Y. H.; Wang, T. H.; Duan, X. C.; Lian, J. B.; Zheng, W. J. NiO Nanomaterials: Controlled Fabrication, Formation Mechanism and The Application in Lithium-Ion Battery. *CrystEngComm* **2012**, *14*, 453−459.
(18) Zhang, P.; Guo, Z. P.; Liu, H. K. Submicron-Sized Cube-Like α-Fe_2O_3 Agglomerates as an Anode Material for Li-Ion Batteries. *Electrochim. Acta* **2010**, *55*, 8521−8526.
(19) Cui, Y. F.; Wang, C.; Wu, S. J.; Liu, G.; Zhang, F. F.; Wang, T. M. Lotus-Root-Like NiO Nanosheets and Flower-Like NiO Microspheres: Synthesis and Magnetic Properties. *CrystEngComm* **2011**, *13*, 4930−4934.
(20) Zhu, L. P.; Xiao, H. M.; Liu, X. M.; Fu, S. Y. Template-Free Synthesis and Characterization of Novel 3D Urchin-Like α-Fe_2O_3 Superstructures. *J. Mater. Chem.* **2006**, *16*, 1794−1797.
(21) Kim, S.-I.; Lee, J.-S.; Ahn, H.-J.; Song, H.-K.; Jang, J.-H. Facile Route to an Efficient NiO Supercapacitor with a Three-Dimensional Nanonetwork Morphology. *ACS Appl. Mater. Interfaces* **2013**, *5*, 1596−1603.
(22) Chaudhari, S.; Bhattacharjya, D.; Yu, J.-S. 1-Dimensional Porous α-Fe_2O_3 Nanorods as High Performance Electrode Material for Supercapacitors. *RSC Adv.* **2013**, *3*, 25120−25128.
(23) Ni, X. M.; Zhao, Q. B.; Zhou, F.; Zheng, H. G.; Cheng, J.; Li, B. B. Synthesis and Characterization of NiO Strips from a Single Source. *J. Cryst. Growth* **2006**, *289*, 299−302.
(24) Gao, G.; Gao, W. J.; Guo, X. Q.; Wang, H.; Wu, H. X.; Zhang, C. L.; Wang, C.; Cui, D. X. Synthesis of Single-Crystalline α-Fe_2O_3 Nanobelts via a Facile PEG-200 Assisted Solution Route. *CrystEngComm* **2011**, *13*, 6045−6049.
(25) Shi, C. S.; Wang, G. Q.; Zhao, N. Q.; Du, X. W.; Li, J. J. NiO Nanotubes Assembled in Pores of Porous Anodic Alumina and Their Optical Absorption Properties. *Chem. Phys. Lett.* **2008**, *454*, 75−79.
(26) Liu, L.; Kou, H.-Z.; Mo, W. L.; Liu, H. J.; Wang, Y. Q. Surfactant-Assisted Synthesis of α-Fe_2O_3 Nanotubes and Nanorods with Shape-Dependent Magnetic Properties. *J. Phys. Chem. B* **2006**, *110*, 15218−15223.
(27) Qiu, Y. J.; Yu, J.; Tan, C. L.; Yin, J. Preparation of Honeycomb-Like NiO with Nanogrooves by Using Electrospun Nanofibrous Webs as Templates. *Mater. Lett.* **2009**, *63*, 200−202.
(28) Chueh, Y. L.; Lai, M. W.; Liang, J. Q.; Chou, L. J.; Wang, Z. L. Systematic Study of The Growth of Aligned Arrays of α-Fe_2O_3 and Fe_3O_4 Nanowires by a Vapor−Solid Process. *Adv. Funct. Mater.* **2006**, *16*, 2243−2251.
(29) Kavitha, T.; Yuvaraj, H. A Facile Approach to the Synthesis of High-Quality NiO Nanorods: Electrochemical and Antibacterial Properties. *J. Mater. Chem.* **2011**, *21*, 15686−15691.
(30) Wang, Z. Y.; Luan, D. Y.; Madhavi, S.; Li, C. M.; Lou, X. W. α-Fe_2O_3 Nanotubes with Superior Lithium Storage Capability. *Chem. Commun.* **2011**, *47*, 8061−8063.
(31) Liang, Z. H.; Zhu, Y. J.; Hu, X. L. β-Nickel Hydroxide Nanosheets and Their Thermal Decomposition to Nickel Oxide Nanosheets. *J. Phys. Chem. B* **2004**, *108*, 3488−3491.
(32) Chen, J. S.; Zhun, T.; Yang, X. H.; Yang, H. G.; Lou, X. W. Top-Down Fabrication of α-Fe_2O_3 Single-Crystal Nanodiscs and Microparticles with Tunable Porosity for Largely Improved Lithium Storage Properties. *J. Am. Chem. Soc.* **2010**, *132*, 13162−13164.
(33) Kim, H.-J.; Choi, K.-I.; Kim, K.-M.; Na, C. W.; Lee, J.-H. Highly Sensitive C_2H_5OH Sensors Using Fe-Doped NiO Hollow Spheres. *Sens. Actuators, B* **2012**, *171−172*, 1029−1037.
(34) Li, L. L.; Chu, Y.; Liu, Y.; Dong, L. H. Template-Free Synthesis and Photocatalytic Properties of Novel Fe_2O_3 Hollow Spheres. *J. Phys. Chem. C* **2007**, *111*, 2123−2127.
(35) Chen, Y.-C.; Zheng, F.-C.; Min, Y.-L.; Wang, T.; Zhang, Y.-G.; Wang, Y.-X. Facile Procedure to Synthesize Highly Crystalline Ag/NiO Nanocomposite Microspheres and Their Photocatalytic Activity. *J. Mater. Sci.: Mater. Electron.* **2012**, *23*, 1592−1598.
(36) Sun, P.; You, L.; Wang, D. W.; Sun, Y. F.; Ma, J.; Lu, G. Y. Synthesis and Gas Sensing Properties of Bundle-Like α-Fe_2O_3 Nanorods. *Sens. Actuators, B* **2011**, *156*, 368−374.
(37) Sugiyama, I.; Shibata, N.; Wang, Z. C.; Kobayashi, S.; Yamamoto, T.; Ikuhara, Y. Ferromagnetic Dislocations in Antiferromagnetic NiO. *Nat. Nanotechnol.* **2013**, *8*, 266−270.
(38) Wu, P.; Sun, J. H.; Huang, Y. Y.; Gu, G. F.; Tong, D. G. Solution Plasma Synthesized Nickel Oxide Nanoflowers: An Effective NO_2 Sensor. *Mater. Lett.* **2012**, *82*, 191−194.
(39) Bai, G. M.; Dai, H. X.; Deng, J. G.; Liu, Y. X.; Qiu, W. G.; Zhao, Z. X.; Li, X. W.; Yang, H. G. The Microemulsion Preparation and High Catalytic Performance of Mesoporous NiO Nanorods and Nanocubes for Toluene Combustion. *Chem. Eng. J.* **2013**, *219*, 200−208.
(40) Needham, S. A.; Wang, G. X.; Liu, H. K. Synthesis of NiO Nanotubes for Use as Negative Electrodes in Lithium Ion Batteries. *J. Power Sources* **2006**, *159*, 254−257.
(41) Wu, J. L.; Huang, Y. X.; Xia, Q. B.; Li, Z. Decomposition of Toluene in a Plasma Catalysis System with NiO, MnO_2, CeO_2, Fe_2O_3, and CuO Catalysts. *Plasma Chem. Plasma Process.* **2013**, *33*, 1073−1082.